

Effect of the final state interaction of $\eta'N$ on the η' photoproduction off nucleon

Shuntaro Sakai^{1a}, Atsushi Hosaka¹, and Hideko Nagahiro^{1,2}

¹*Research Center for Nuclear Physics (RCNP),*

Osaka University, Ibaraki, Osaka, 567-0047, Japan.

²*Department of Physics, Nara Womens's University, Nara 630-8506, Japan.*

(Dated: December 9, 2024)

Abstract

We investigate the η' photoproduction off the nucleon with a particular interest in the effect of the final-state interaction (FSI) of the η' meson and nucleon ($\eta'N$) based on three-flavor linear sigma model. We find an enhancement in the cross section of the η' photoproduction near the $\eta'N$ -threshold energy owing to the $\eta'N$ FSI. With the η' meson at forward angles, the energy dependence near the $\eta'N$ threshold is well reproduced with the $\eta'N$ FSI. The cross section at backward angles can also be a good probe to investigate the strength of the $\eta'N$ interaction.

^a shsakai@rcnp.osaka-u.ac.jp

I. INTRODUCTION

Hadrons are elementary excitations of the vacuum of quantum chromodynamics (QCD), and their properties reflect the vacuum structure of the low-energy QCD. The chiral symmetry is a basic feature of QCD, and it is broken spontaneously at low energies. In the nuclear medium, the spontaneously broken symmetry is expected to be restored, which we call chiral restoration, and the possible change of hadron properties associated with the chiral restoration at finite baryon densities has been an important subject of hadron physics (see, for example, Ref. [1] for a recent review article). For example, some theoretical analyses suggest the mass reduction of vector mesons as an evidence of the restoration of the chiral symmetry [2]. Attempts and discussions have been proposed for the study of vector mesons in nuclear medium from the theoretical and experimental sides up to now [3]. The analyses of the pion-nucleus system suggest partial restoration of chiral symmetry in the nuclear medium; the pion decay constant, the order parameter of the spontaneous breaking of chiral symmetry, is expected to be reduced about 35% at the normal nuclear density [4–7].

The pseudoscalar meson η' is another candidate to probe such a change of the vacuum property. Its mass is larger than other low-lying pseudoscalar mesons, such as π , K , or η , due to the chiral symmetry breaking in the three-flavor system [8–14] together with the $U_A(1)$ anomaly in QCD [15]. A simple estimation taking into account the restoration of chiral symmetry suggests as large as 150 MeV reduction of the η - η' mass difference in the nuclear medium at the normal nuclear density even if the property of the $U_A(1)$ anomaly is unchanged in the medium [16], while there are some theoretical and experimental studies suggesting the change of the η' properties in medium from the effective restoration of the $U_A(1)$ symmetry [8, 9, 17, 18]. In addition, mass reduction of the η' meson in the nuclear medium has been obtained also in some theoretical analyses [19–22], and there exist some experimental studies [23–25]. Theoretical studies have been performed for the formations of η' -nucleus ($\eta'A$) bound state [20, 26–29], where they have demonstrated that the spectrum may show clear peak structure if the $\eta'A$ interaction is attractive and if the absorption into nucleus is small enough to accommodate narrow η' bound states to the nucleus. From the experimental side, the analyses of the η' transparency ratio suggest a small imaginary part of the η' optical potential [24, 30].

By now there are several theoretical investigations for the two-body interaction between

the η' meson and nucleon ($\eta'N$) which is a key information of the η' properties in the nuclear medium [21, 22, 31–36]. So far, the $\eta'N$ interaction is not known well despite some experimental attempts [37, 38]. In this work, we investigate the η' photoproduction off a free nucleon with the final-state interaction (FSI) between the η' meson and nucleon in a three-flavor linear sigma model. In the model, the strongly attractive $\eta'N$ interaction is dictated by the $U_A(1)$ anomaly and the scalar-meson exchange, and an $\eta'N$ bound state is generated with a binding energy of typically about a few ten MeV [21, 35]. The η' photoproduction off the nucleon has been intensively studied theoretically [39] and experimentally at photon facilities such as JLab, Mainz, Bonn, SPring-8 and so on [40–44]. There, the importance of the ρ meson exchange in the t channel is pointed out. In the present study, we supplement the ρ meson in the linear sigma model with relevant couplings fixed by existing data. We then focus on the final-state interaction of the η' meson with the nucleon which can affect the energy dependence of the production cross sections near and above the threshold. Our results in turn imply that such a study is useful to extract the $\eta'N$ interaction from experimental data.

This paper is organized as follows. In Sec. II, we explain the model setup used in this analysis of the η' photoproduction. The $\eta'N$ interaction and the photoproduction amplitude used in the present study are also explained in this section. Section III is devoted to the discussion of the cross section and the beam asymmetry of the η' photoproduction off the nucleon with the inclusion of the $\eta'N$ FSI. The summary and outlook of this study is given in Sec. IV.

II. FORMULATION

A. Model Lagrangian

In this section, we explain the model setup for the η' photoproduction in the three-flavor linear sigma model. In the linear model hadrons including pseudoscalar mesons, scalar mesons, and baryons are introduced as linear representations of chiral symmetry and their interactions are determined. This is done first by constructing a chiral invariant Lagrangian and then the vacuum is determined to minimize the effective potential; the neutral scalar fields have non-zero expectation values in association with the chiral symmetry breaking.

Hadron properties in such a framework can naturally be related to the vacuum structure.

The Lagrangian used in this calculation is given by,

$$\begin{aligned}
\mathcal{L} &= \mathcal{L}_M + \mathcal{L}_N + \mathcal{L}_{\gamma VP}, \tag{1} \\
\mathcal{L}_M &= \frac{1}{2} \text{tr} [D_\mu M (D^\mu M)^\dagger] - \frac{\mu^2}{2} \text{tr} [MM^\dagger] - \frac{\lambda}{4} \text{tr} [(MM^\dagger)^2] - \frac{\lambda'}{4} [\text{tr} (MM^\dagger)]^2 \\
&\quad + \sqrt{3} B (\det M + \det M^\dagger) + A \text{tr} (\chi M^\dagger + M \chi^\dagger) \\
&\quad - \frac{1}{4} \text{tr} [(L^{\mu\nu})^2 + (R^{\mu\nu})^2] + \frac{m_0^2}{2} \text{tr} [(L^\mu)^2 + (R^\mu)^2], \\
\mathcal{L}_N &= \bar{N} \left[i \left\{ \not{\partial} + i g_V \left(\not{V} + \frac{\kappa_V}{2m_N} \sigma_{\mu\nu} \partial^\mu V^\nu \right) \right\} \right. \\
&\quad \left. - m_N - g \left\{ \left(\frac{\tilde{\sigma}_0}{\sqrt{3}} + \frac{\tilde{\sigma}_8}{\sqrt{6}} \right) + i \gamma_5 \left(\frac{\eta_0}{\sqrt{3}} + \frac{\vec{\pi} \cdot \vec{\tau}}{\sqrt{2}} + \frac{\eta_8}{\sqrt{6}} \right) \right\} \right] N \\
\mathcal{L}_{\gamma VP} &= e g_{\gamma V^a P} \epsilon^{\mu\nu\alpha\beta} (\partial_\mu V_\nu^a) (\partial_\alpha A_{\text{em}\beta}) \eta', \\
D_\mu M &= \partial_\mu M + i g_V (L_\mu M - M R_\mu^\dagger), \\
M &= M_s + i M_{ps} = \sum_{a=0}^8 \frac{\sigma^a \lambda^a}{\sqrt{2}} + i \sum_{a=0}^8 \frac{\pi^a \lambda^a}{\sqrt{2}}, \\
N &= {}^t(p, n), V^\mu = \frac{1}{\sqrt{2}} \sum_{a=0}^3 \frac{V^{a\mu} \tau^a}{\sqrt{2}}, \\
\chi &= \sqrt{3} \text{diag}(m_u, m_d, m_s) = \sqrt{3} \text{diag}(m_q, m_q, m_s),
\end{aligned}$$

where we write L^μ and R^μ as $L^\mu = V^\mu + A^\mu$ and $R^\mu = V^\mu - A^\mu$ using the vector and the axial-vector fields V^μ and A^μ , and $e > 0$ is the elementary charge unit. A_{em}^μ denotes the electromagnetic field. $\tilde{\sigma}_i$ ($i = 0, 8$) appearing in the nucleon part is the fluctuation of the neutral scalar field from its mean field. The mean field is determined so as to minimize the effective potential, which is obtained in the tree-level approximation in this study. The isospin symmetry is implemented with the degenerate u and d quark masses. The Lagrangian except for the vector field is the same as that used in Refs. [21, 35].

The Lagrangian is constructed to be invariant under the chiral transformation for the hadron field. The meson field M is transformed as $U_L M U_R^\dagger$ with $U_{L/R}$ the element of $\text{SU}(3)_{L/R}$. Here, we note that the term proportional to B , which is not invariant under the $U_A(1)$ transformation, reflects the effect of the $U_A(1)$ anomaly. For the fermion part, the irrelevant hyperons in this study are omitted. The values of various coupling constants in the Lagrangian are summarized in Table I. The coupling of the vector meson and nucleon g_V is fixed with the Kawarabayashi-Suzuki-Fayyazuddin-Riazuddin relation $g_V = \frac{m_V}{\sqrt{2}f}$ [45], where

TABLE I. Values of the parameters in the Lagrangian.

$g_V[-]$	$\kappa_\rho[-]$	$\kappa_\omega[-]$	$g_{\gamma\eta'\rho}[\text{MeV}^{-1}]$	$g_{\gamma\eta'\omega}[\text{MeV}^{-1}]$	$g[-]$
5.95	3.586	0	1.625×10^{-3}	5.622×10^{-4}	7.698

m_V and f are $m_V = (m_\rho + m_\omega)/2$ and $f = 92.2$ MeV. The masses of the ρ and ω mesons are taken from Ref. [46]. The coefficient of the Pauli coupling between the nucleon and vector meson κ_V is determined to reproduce the anomalous magnetic moment of proton, $\kappa_p = 1.793$. Following Refs. [21, 35], the parameter g in the nucleon part is determined for $\langle\sigma\rangle$, the chiral order parameter, to reduce 35% at the normal nuclear density which is suggested by the analysis of the pion-nucleus system [4]. For the masses of the η , η' mesons and the nucleon, there are constraints in our model. However, in the present study of the η' photoproduction, we employ the experimental values for these masses. The coupling of the photon γ , vector meson V^a ($V^0 = \omega$ and $V^3 = \rho^0$), and the η' meson is called the anomalous coupling which is induced by the chiral anomaly in QED [47] with the vector meson dominance. Here, we use $g_{\gamma V^a \eta'}$ determined from the observed partial width of the η' radiative decay [46].

B. $\eta'N$ amplitude for FSI

In this section, we briefly revisit the $\eta'N$ amplitude in the framework of the linear sigma model [21, 35], which is relevant to the purpose of this study. The η' photoproduction amplitude is given by the T matrix $T_{\gamma N \rightarrow \eta' N}$ as

$$T_{\gamma N \rightarrow \eta' N} = V_{\gamma N \rightarrow \eta' N}(1 + G_{\eta' N} T_{\eta' N \rightarrow \eta' N}), \quad (2)$$

whose diagrammatic expression is shown in Fig. 1. In Eq. (2), $V_{\gamma N \rightarrow \eta' N}$, $G_{\eta' N}$, and $T_{\eta' N \rightarrow \eta' N}$ are the η' -photoproduction kernel, the $\eta'N$ two-body Green's function, and the $\eta'N$ T matrix, respectively. The amplitude $T_{\eta' N \rightarrow \eta' N}$ is responsible for the rescattering of the η' meson and nucleon in the final state. The T matrix is obtained from a two-channel coupled equation of $\eta'N$ ($i = 1$) and ηN ($i = 2$). With the interaction kernels of the $\eta'N$ and ηN channels

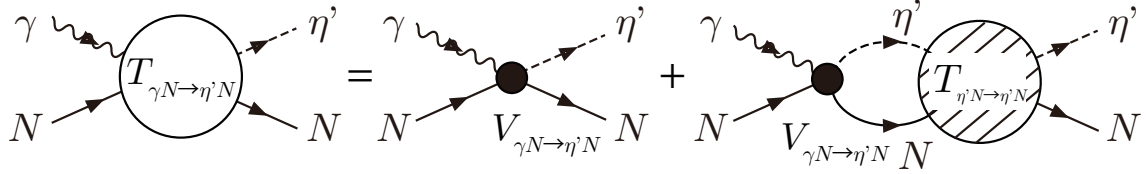


FIG. 1. Diagrams for the scattering equation Eq. (2) for the η' -photoproduction T matrix. The white, small black, and shaded blobs are the T matrix of the η' photoproduction, $T_{\gamma N \rightarrow \eta' N}$, the η' -photoproduction vertex, $V_{\gamma N \rightarrow \eta' N}$, and the $\eta' N$ T matrix, $T_{\eta' N \rightarrow \eta' N}$. The solid, dashed, and wavy lines stand for the propagations of the nucleon, η' meson, and photon, respectively.

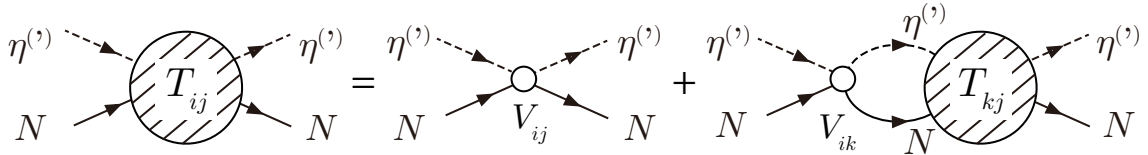


FIG. 2. A diagrammatic representation of the scattering matrix for the $\eta' N$ scattering including the $\eta' N$ and ηN channels, T_{ij} ($i, j = \eta' N, \eta N$). The shaded and small white blobs represent the T matrices, T_{ij} , and interaction kernels, V_{ij} . The solid line denotes the propagation of the nucleon, and the dashed one represents that of the η or η' meson.

V_{ij} ($i, j = 1, 2$), the T matrices T_{ij} satisfy the scattering equation given by,

$$T_{ij} = V_{ij} + V_{ik} G_k T_{kj}, \quad (3)$$

where

$$V_{11} = -\frac{6gB}{\sqrt{3}m_{\sigma_0}^2}, V_{12} = V_{21} = +\frac{6gB}{\sqrt{6}m_{\sigma_8}^2}, V_{22} = 0. \quad (4)$$

The diagrammatic expression of Eq. (3) is given in Fig. 2. The interaction kernels V_{ij} given in Eq. (4) are obtained from the scattering amplitude within the tree-level approximation and the leading order of the momentum expansion in the flavor $SU(3)$ symmetric limit. The diagrams taken into account in this calculation are shown in Fig. 3, where the scalar-meson

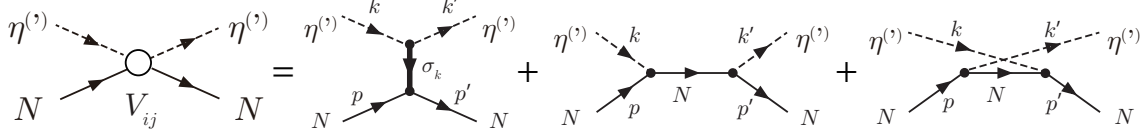


FIG. 3. Diagrams for the interaction kernels V_{ij} in Eq. (3) at the tree level. The thick solid line stands for the propagation of the scalar meson, and the other lines have the same notations as those in Fig. 2. The first term is the contribution from the scalar-meson exchange in the t channel, and the second and third ones represent the Born terms in the s and u channels, respectively.

exchange in the t channel and the Born diagrams in the s and u channels are considered. One can see in Eq. (4) that an attractive interaction between the η' meson and nucleon is induced by the scalar-meson exchange in this approximation. It is noteworthy that this interaction kernel is proportional to B , which reflects the effect of the $U_A(1)$ anomaly as we mentioned in Sec. II A. Owing to this attraction, the bound state of the η' meson and nucleon can be generated. In this study, the vector-meson contribution for the $\eta'N$ interaction is not taken into account, because they do not give the leading contribution in the momentum expansion. Here, we take account of the $\eta'N$ and ηN channels, and omit the πN one, because we expect that the contribution from the πN channel would be small owing to the smallness of the $\pi N \rightarrow \eta'N$ cross section [48]. The divergence contained in the two-body Green's function G_i is removed by the dimensional regularization and the subtraction constant is fixed with the natural renormalization scheme [49]. The relevant parameters are given as $B = 997.95$ MeV, $g = 7.698$, $m_{\sigma_0} = 700$ MeV, $m_{\sigma_8} = 1225$ MeV, and the subtraction constants are $a_{\eta'N}(\mu = m_N) = -1.838$ and $a_{\eta N}(\mu = m_N) = -1.239$, where μ is the renormalization point. We use the same subtraction constant appearing in the Green's function in Eq. (2) as that in the $\eta'N$ T matrix in Eq. (3).

For the purpose of seeing the effect of the $\eta'N$ FSI, we show the result with varying the parameter g as (a) $g \times 0.0$, (b) 1.0, (c) 0.5, (d) 1.5, and (e) -0.5 . The coupling strength, $\eta'N$ scattering length, and binding energy of the $\eta'N$ bound state in these cases are summarized in Table II.

TABLE II. Table for the coupling strength, scattering length, and binding energy for the cases (a) to (e). The cases (a) to (e) are characterized by the coupling parameter g .

	(a)	(b)	(c)	(d)	(e)
coupling strength	$g \times 0.0$	$g \times 1.0$	$g \times 0.5$	$g \times 1.5$	$g \times -0.5$
scattering length [fm]	0.0	$-1.9 + 0.58i$	$+0.53 + 0.042i$	$-0.77 + 0.086i$	$-0.13 + 2.8 \times 10^{-3}i$
binding energy [MeV]	–	$9.79 - 7.10i$	–	$98.6 - 24.6i$	–

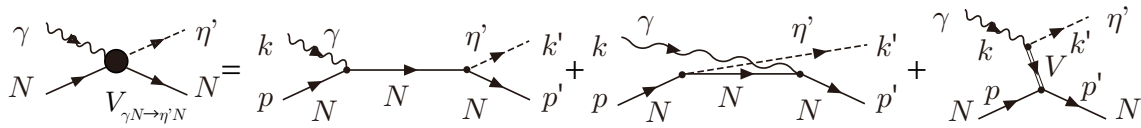


FIG. 4. Diagrams for the η' photoproduction amplitude with the tree-level approximation, with the same notation as in Fig. 1. The first, second, and third terms are the contributions from the s , u , and t channels, respectively.

C. Photoproduction amplitude

In this section, we explain the η' -photoproduction kernel $V_{\gamma N \rightarrow \eta' N}$ in Eq. (2). It is evaluated within the tree-level approximation shown in Fig. 4, which contains the Born diagrams in the s and u channels, and the vector-meson exchange one in the t channel. We can write down the amplitude from these diagrams as follows;

$$\begin{aligned}
 -i\mathcal{M}_{\text{tree}} = & e\bar{u}(p', s') \left[g_{PN} \left\{ \gamma_5 \frac{F_s \not{k} + F_c (\not{p} + m_N)}{(p+k)^2 - m_N^2} \not{\epsilon} + \not{\epsilon} \frac{-F_u \not{k}' + F_c (\not{p} + m_N)}{(p-k')^2 - m_N^2} \gamma_5 \right. \right. \\
 & \left. \left. + \frac{\kappa_p}{4m_N} \left(F_s \gamma_5 \frac{\not{p} + \not{k} + m_N}{(p+k)^2 - m_N^2} [\not{k}, \not{\epsilon}] + F_u [\not{k}, \not{\epsilon}] \frac{\not{p} - \not{k}' + m_N}{(p-k')^2 - m_N^2} \gamma_5 \right) \right\} \\
 & \left. + iF_t \frac{g_V g_{\gamma V^a P} / 2}{t - m_V^2 + i\epsilon} g_{\mu\sigma} \epsilon^{\rho\sigma\alpha\beta} k'_\rho k_\alpha \epsilon_\beta \left\{ \gamma^\mu + \frac{\kappa_{V^a}}{4m_N} [\not{q}, \gamma^\mu] \right\} \right] u(p, s), \quad (5)
 \end{aligned}$$

where ϵ^μ is the polarization vector of the photon, and the momentum transfer q^μ is written as $q^\mu = p'^\mu - p^\mu$. Here, the form factors F_x ($x = s, t, u$) are introduced in a gauge invariant manner following Ref. [50] and references therein. The form factors F_x appearing in Eq. (5) are written as $F_x = \Lambda_x^4 / ((x - m_x^2)^2 + \Lambda_x^4)$, and F_c is given as $F_c = F_s + F_u - F_s F_u$, where m_x denotes the exchanged hadron mass in the channel x . The form factor reflects the size of hadron, and the typical value of the cutoff parameter Λ_x is about 1 GeV. We will discuss the

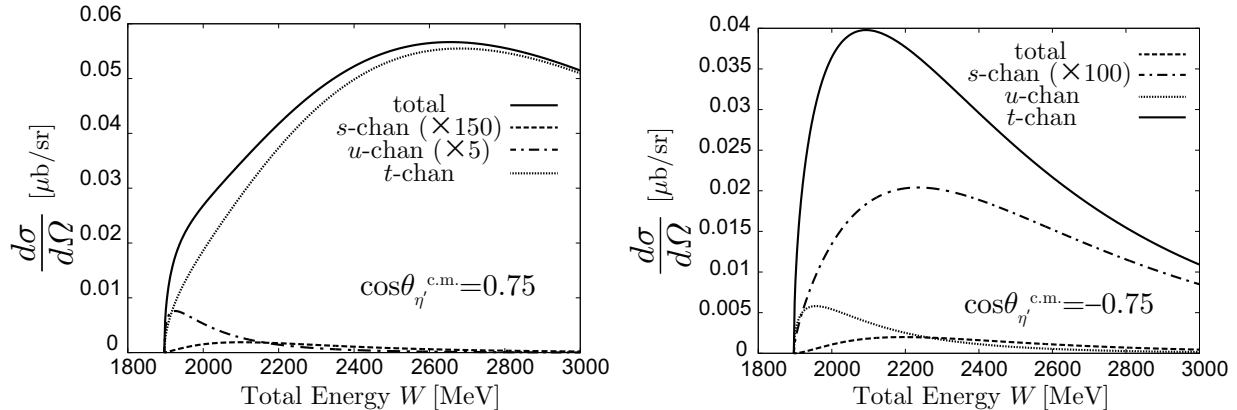


FIG. 5. Differential cross sections of the η' photoproduction without FSI at $\cos\theta_{\eta'}^{\text{c.m.}} = 0.75$ (left) and -0.75 (right) as functions of the total energy W in the c.m. frame. In the left figure, s - and u -channel contributions are multiplied by factors 150 and 5, respectively, and the s -channel one in the right figure is multiplied by a factor 100.

actual values in the next section. For the kernel $V_{\gamma N \rightarrow \eta' N}$ in Eq. (2), we use the production amplitude $\mathcal{M}_{\text{tree}}$ in Eq. (5) by factorizing the amplitude with its on-shell value.

In the present calculation, we have omitted the direct production of the η meson from the photon $V_{\gamma N \rightarrow \eta N}$, expecting that the energy dependence of that channel is not very large in the region of the $\eta' N$ threshold because the pole position of $N^*(1535)$, which has the dominant contribution for the η -meson photoproduction, is far from there.

III. RESULT

Let us first discuss differential cross sections of the η' photoproduction without the $\eta' N$ FSI as functions of the total energy W in the center-of-mass (c.m.) frame. The results are shown in Fig. 5. The left and right panels of the figure correspond to the cases of an η' meson production at the forward angle ($\cos\theta_{\eta'}^{\text{c.m.}} = 0.75$) and the backward one ($\cos\theta_{\eta'}^{\text{c.m.}} = -0.75$), respectively, where $\theta_{\eta'}^{\text{c.m.}}$ denotes the angle between the initial photon and the produced η' meson in the c.m. frame. For the cutoff parameters, we use $\Lambda = \Lambda_x = 700$ MeV ($x = s, t, u$). In this figure, separate contributions from the s , t , and u channels are plotted. From the left panel of Fig. 5, we find that the cross section at the forward angle is dominated by the t -channel contribution with the vector-meson exchange. On the other hand, the u -channel contribution of the second term of Fig. 4 has a large fraction at the backward angle.

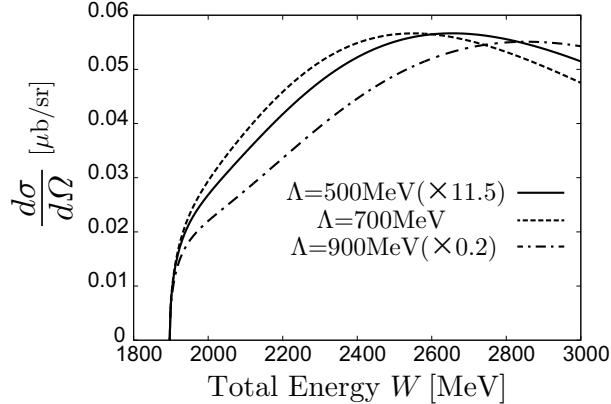


FIG. 6. Cutoff dependence of the differential cross sections of the η' photoproduction off the nucleon without the $\eta'N$ FSI. The cutoff parameter Λ is varied as $\Lambda = 500, 700,$ and 900 MeV. Note that the results for $\Lambda = 500$ and 900 MeV are scaled by factors 11.5 and 0.2, respectively.

As is often the case, the reaction cross sections depend on the cutoff parameters of the form factor. Thus in Fig. 6 we show the differential cross sections at the forward angle with varying the cutoff parameter as $\Lambda = 500, 700,$ and 900 MeV without the $\eta'N$ FSI. With the introduction of the form factor, some characteristic peak structure may appear in the energy dependence of cross section due to the competition of the increasing behavior of the phase space volume and the decreasing behavior of the form factor as the energy (or the relative momentum q) is increased. The cross section is proportional to $q|F(q)|^2$, where q is the relative momentum of the final state $\eta'N$, and is related to the kinetic energy E by $E = q^2/2\mu$ in the non-relativistic approximation for small q (μ is the reduced mass). By using the typical cutoff $\Lambda \sim 1$ GeV and $\mu \sim 0.5$ GeV for the $\eta'N$ system, we find the peak position at around some hundreds MeV above the threshold. In Fig. 6, one finds that there is a peak at 2.5-2.8 GeV, that is, 600-900 MeV above the $\eta'N$ threshold as we expected, and that any characteristic structure around the threshold does not appear with these cutoff parameters.

Now, Fig. 7 shows the total energy W dependence of the differential cross sections with the inclusion of the $\eta'N$ FSI. The strength of the $\eta'N$ interaction is varied by changing the parameter g appearing in Eq. (4) to see the dependence on the strength of the $\eta'N$ FSI. In the figure, the cases (a) to (e) correspond to those explained in Sec. II B; (a) without FSI; (b), (c), (d) with attractive FSI; and (e) with repulsive FSI. Here, we use the same value for the cutoff parameter $\Lambda = 700$ MeV in all cases (a) to (e). In this study, only the $\eta'N$ FSI

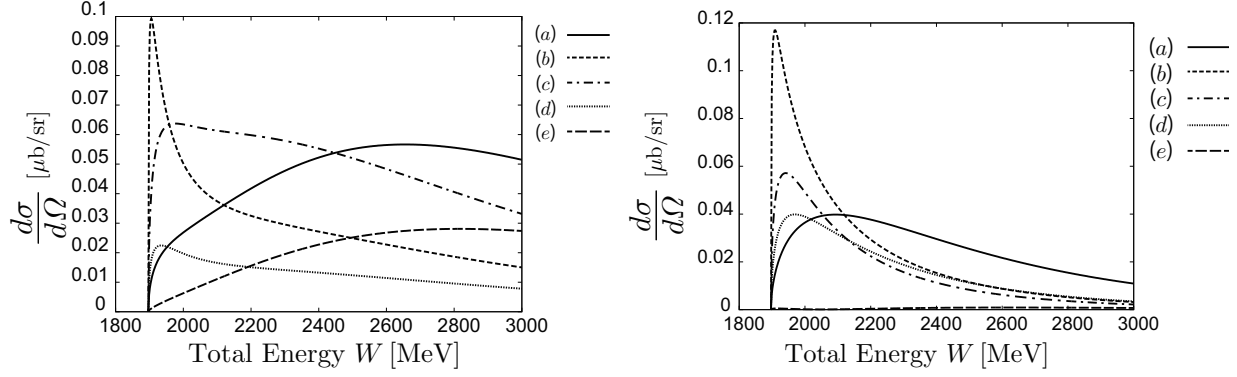


FIG. 7. Differential cross sections at the forward (left, $\cos\theta_{\eta'}^{\text{c.m.}} = 0.75$) and the backward (right, $\cos\theta_{\eta'}^{\text{c.m.}} = -0.75$) angles as functions of W with and without the $\eta'N$ FSI. The cases (a) to (e) in the legend follow those given in Table II.

in the S-wave part is included. Therefore, we mainly focus on the energy around the $\eta'N$ threshold in the following discussions.

In the left panel of Fig. 7 for the forward production of the η' meson, we find a broad bump structure around 2.6 GeV for the case (a) without FSI, which originates from the form factor as mentioned above. With the inclusion of the $\eta'N$ FSI, the structure is modified: In the case (b), a significant enhancement near the $\eta'N$ threshold appears, which stems from the existence of a bound state just below the threshold. The enhancement becomes more moderate in the cases (c) and (d), where there exists no bound state around the $\eta'N$ threshold. Thus, we find an enhancement of the forward cross section near the $\eta'N$ threshold due to the attractive $\eta'N$ FSI. In the case (e), where the $\eta'N$ FSI is repulsive, one cannot find such an enhancement. When the η' meson is emitted at the backward angle, the $\eta'N$ FSI gives similar effect on the energy dependence of the cross sections as shown in the right panel of Fig. 7; the larger cross sections near the $\eta'N$ threshold are obtained in the cases (b), (c), and (d) than that in the case (a), and one can see the suppression in the case (e) compared with the case (a).

In Fig. 8, we show the result of the differential cross sections compared with the experimental data [40]. In doing so, we have tuned the cutoff parameters $\Lambda_{u,s}$ and Λ_t for each strength of the $\eta'N$ FSI to make an optimal comparison with the experimental data near the threshold at both forward and backward angles. The resulting cutoff parameters Λ_x are summarized in Table III. At the forward angle shown in the left panel of Fig. 8, the

TABLE III. Cutoff parameters Λ_x used for the results shown in Fig. 8 in units of MeV. The cases (a) to (e) follow those of Table II.

	(a)	(b)	(c)	(d)	(e)
$\Lambda_{s,u}$	600	680	680	650	0
Λ_t	750	610	650	790	840

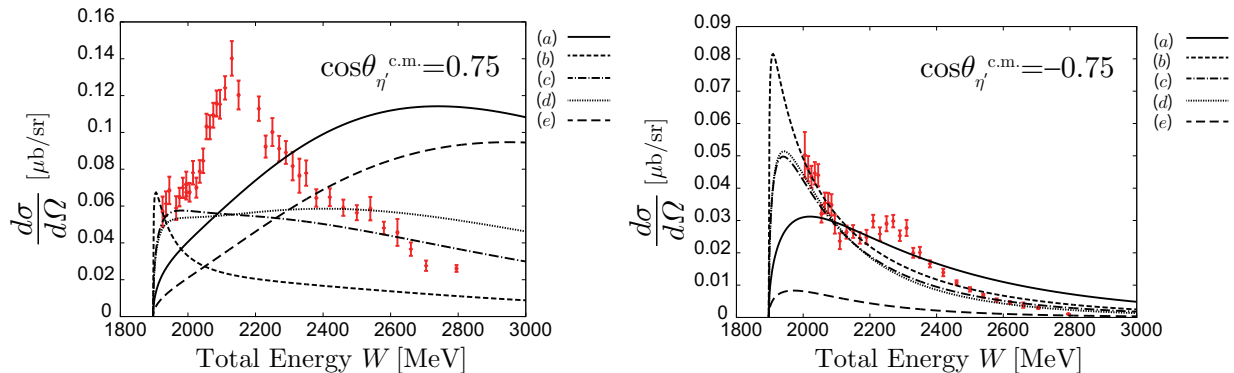


FIG. 8. Differential cross sections of the η' photoproduction at $\cos\theta_{\eta'}^{c.m.} = 0.75$ (left) and -0.75 (right) as functions of the total energy W . The cases (a) to (e) in the legend are the same as those in Fig. 7. The points with the error bar are the experimental data taken from Ref. [40].

rapid increase near the threshold is well reproduced in the cases (b), (c), and (d), where the $\eta'N$ FSI is attractive, though such behavior is not seen in the cases without the $\eta'N$ FSI, (a), nor with the repulsive one, (e). In the present method, we cannot reproduce a broad peak at around $W = 2.1$ GeV in the experimental data, which is considered to be due to a resonance as discussed in Ref. [39]. In the present study, however, we do not consider the resonance in that energy region, and we rather focus our discussions on the near threshold behavior by the $\eta'N$ FSI.

Next, we move to the backward production of the η' meson given in the right panel of Fig. 8. Here, we note that the experimental data in Ref. [40] very near the $\eta'N$ threshold are missing, and that only the data above 2 GeV are available. We find a clear effect of the FSI at the total energy W below 2 GeV. The attractive $\eta'N$ FSI, the cases (b), (c), and (d), leads to a rapid increase of the cross sections around the $\eta'N$ -threshold energy. In the case (e), the cross section is smaller than that in the case (a). This difference of the cross

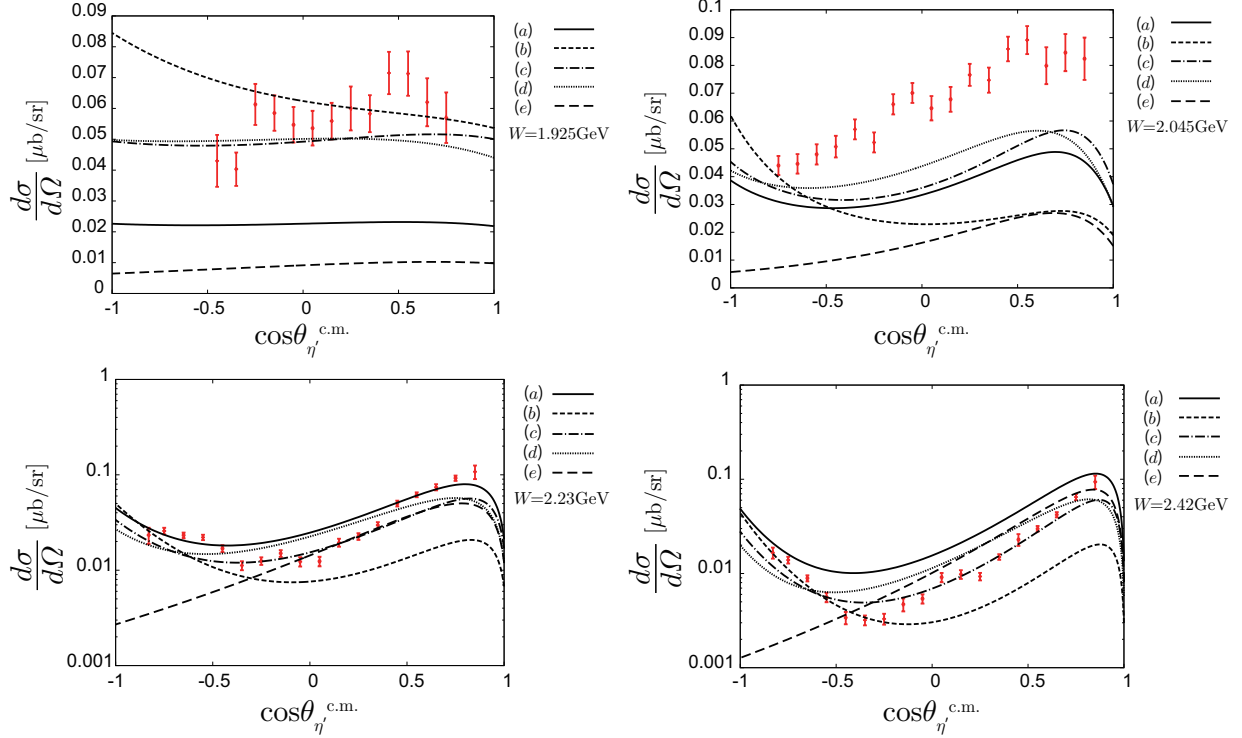


FIG. 9. Differential cross section of the η' photoproduction as functions of $\cos\theta_{\eta'}^{\text{c.m.}}$ with and without the $\eta'N$ FSI at $W = 1.925$ (upper left), 2.045 (upper right), 2.230 (lower left), and 2.420 (lower right) GeV. The legend is the same as that in Fig. 7.

sections near the $\eta'N$ threshold can be a probe to investigate the strength of the low-energy $\eta'N$ interaction. As corresponding to the broad peak seen in the experimental data at the forward angle, a dip-like structure is seen at the backward angle at the same energy region $W \sim 2.1$ GeV. Once again, we do not discuss this structure because it may come from the resonance effect as mentioned above.

The differential cross sections at $W = 1.925$, 2.045 , 2.230 , and 2.420 GeV as functions of $\cos\theta_{\eta'}^{\text{c.m.}}$ are shown in Fig. 9. Around the $\eta'N$ -threshold energy, $W = 1.925$ GeV, the cross sections of our calculation do not depend on the variable $\cos\theta_{\eta'}^{\text{c.m.}}$ so much due to the expected S-wave dominance, though the experimental data have some structure. As we mentioned above, the differences among the theoretical curves come from those in the strength of the $\eta'N$ FSI; in the cases (b), (c), and (d) which contain the attractive $\eta'N$ FSI, the cross sections near the $\eta'N$ threshold have larger values compared with that in the case (a). At $W = 2.045$ GeV and around $\cos\theta_{\eta'}^{\text{c.m.}} = 1$, there is discrepancy between our calculation and the experimental data. This energy corresponds to the peak around 2.1

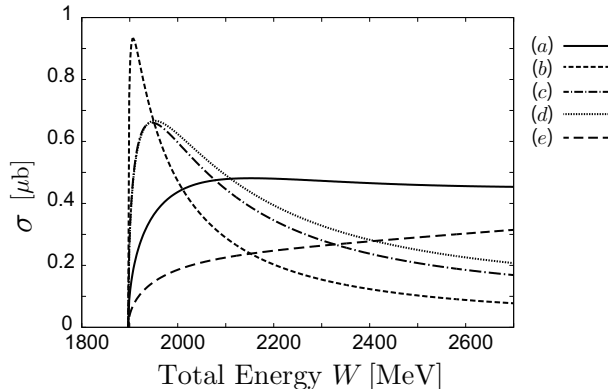


FIG. 10. Total cross sections of the η' photoproduction off the nucleon as functions of the total energy W . The legend is the same as that in Fig. 7.

GeV in the experimental data in Fig. 8, which may come from the resonance contribution as mentioned above. At higher energies ($W = 2.23$ and 2.42 GeV), the forward peak structure stemming from the t -channel contribution becomes more apparent. The difference of the behavior at the backward angle is caused by that of the u -channel contribution associated with the change of the parameter g .

In Fig. 10, we show the total cross sections of the η' photoproduction as functions of the total energy W . As in the case of the differential cross section, the enhancement of the cross sections near the $\eta'N$ threshold is seen in the cases (b), (c), and (d) with the attractive $\eta'N$ FSI. In the case (e), the cross section is smaller than that in the case (a).

Finally, we show the beam asymmetries Σ against the scattering angle $\theta_{\eta'}^{c.m.}$. Σ is defined as

$$\Sigma = \left(\left. \frac{d\sigma}{d\Omega} \right|_{\phi=\pi/2} - \left. \frac{d\sigma}{d\Omega} \right|_{\phi=0} \right) / \left(\left. \frac{d\sigma}{d\Omega} \right|_{\phi=\pi/2} + \left. \frac{d\sigma}{d\Omega} \right|_{\phi=0} \right), \quad (6)$$

where ϕ is the azimuthal angle from the polarization vector of the photon in the initial state. The positive values of the beam asymmetries originate from the dominant contribution of the t -channel diagram, which is of the magnetic nature associated with the anomalous coupling of $\gamma\eta'\rho$. The behavior of the beam asymmetry is qualitatively different from observed one [41]. The difference may come from the interference as pointed out in Ref. [41]. Then, further development of the model, such as, the inclusion of the higher partial-wave contribution may be necessary for the description of the beam asymmetry.

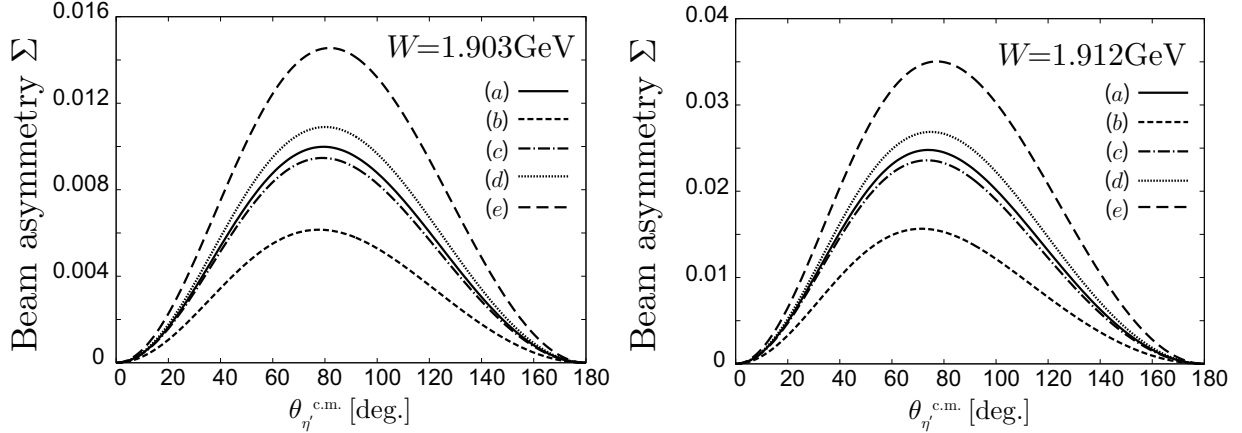


FIG. 11. Beam asymmetries Σ as functions of the scattering angle $\theta_{\eta'}^{\text{c.m.}}$ with the total energy $W = 1.903$ (left) and 1.912 (right) GeV. The cases (a) to (e) in the legend are the same as those in Fig. 7.

IV. SUMMARY AND OUTLOOK

In this paper, we investigated the η' photoproduction off a nucleon with the inclusion of the final-state interaction between the η' meson and nucleon based on the linear sigma model. When there is an attractive final-state interaction, we found an enhancement of the differential cross section near the $\eta'N$ threshold, typically around or below 2 GeV, at the forward and backward angles ($\cos\theta_{\eta'}^{\text{c.m.}} = \pm 0.75$). With an attractive $\eta'N$ interaction, the energy dependence of the cross section near the $\eta'N$ threshold is reproduced fairly well. Particularly, the magnitude of the enhancement near the threshold in the backward production of the η' meson seems to be sensitive to the strength of the $\eta'N$ interaction. The angular dependence of the differential cross section also agrees with the experimental data in Ref. [40]. The enhancement around the $\eta'N$ threshold appears also in the energy dependence of the total cross section. Therefore, precise analysis of the threshold behavior is useful to determine the $\eta'N$ interaction. Despite these agreements, the angular dependence of the beam asymmetry shows qualitatively different behavior as in the previous theoretical calculations [41].

The present study was based on a rather simple model and on the S-wave scattering. Other ingredients such as coupled channels of, e.g., ηN and πN , higher partial waves, resonances, and so on, may be included. These are expected to improve the aspects that

cannot be explained in the present study.

ACKNOWLEDGMENTS

This work is supported in part by the Grants-in-Aid for Science Research (C) by the MEXT (Grant No. JP26400273 for A. H. and No. JP26400275 for H. N.).

- [1] R. S. Hayano and T. Hatsuda, *Rev. Mod. Phys.* **82** (2010) 2949.
- [2] G. E. Brown and M. Rho, *Phys. Rev. Lett.* **66** (1991) 2720.
T. Hatsuda and S. H. Lee, *Phys. Rev. C* **46** (1992) no.1, R34.
- [3] M. Naruki *et al.*, *Phys. Rev. Lett.* **96** (2006) 092301.
P. Gubler and W. Weise, *Nucl. Phys. A* **954** (2016) 125.
- [4] K. Suzuki *et al.*, *Phys. Rev. Lett.* **92** (2004) 072302.
- [5] E. Friedman *et al.*, *Phys. Rev. Lett.* **93** (2004) 122302.
- [6] E. E. Kolomeitsev, N. Kaiser and W. Weise, *Phys. Rev. Lett.* **90** (2003) 092501.
- [7] D. Jido, T. Hatsuda and T. Kunihiro, *Phys. Lett. B* **670** (2008) 109.
- [8] R.D. Pisarski and F. Wilczek, *Phys. Rev.* **D29**, 338 (1984).
- [9] H. Kikuchi and T. Akiba, *Phys. Lett. B* **200** (1988) 543.
- [10] T. Kunihiro and T. Hatsuda, *Phys. Lett. B* **206** (1988) 385 Erratum: [*Phys. Lett.* **210** (1988) 278].
- [11] T. D. Cohen, *Phys. Rev. D* **54** (1996) 1867.
- [12] S.H. Lee and T. Hatsuda, *Phys. Rev.* **D54**, (1996) 1871.
- [13] N. J. Evans, S. D. H. Hsu and M. Schwetz, *Phys. Lett. B* **375** (1996) 262.
- [14] M. C. Birse, T. D. Cohen and J. A. McGovern, *Phys. Lett. B* **388** (1996) 137.

- [15] W.A. Bardeen, Phys. Rev. **184**, 1848 (1969).
M. Kobayashi and T. Maskawa, Prog. Theor. Phys. **44** (1970) 1422.
J. Schechter and Y. Ueda, Phys. Rev. D **3** (1971) 168.
G. 't Hooft, Phys. Rev. D **14** (1976) 3432 Erratum: [Phys. Rev. D **18** (1978) 2199].
E. Witten, Nucl. Phys. B **156**, 269 (1979).
G. Veneziano, Nucl. Phys. B **159**, 213 (1979).
C. Rosenzweig, J. Schechter and C. G. Trahern, Phys. Rev. D **21** (1980) 3388.
- [16] D. Jido, H. Nagahiro and S. Hirenzaki, Phys. Rev. C **85** (2012) 032201.
- [17] T. Kunihiro, Phys. Lett. **B219**, 363 (1989).
- [18] J.I. Kapusta, D. Kharzeev, and L.D. McLerran, Phys. Rev. **D53**, 5028 (1996).
T. Csorgo, R. Vertesi and J. Sziklai, Phys. Rev. Lett. **105** (2010) 182301.
S. Benic, D. Horvatic, D. Kekez and D. Klabucar, Phys. Rev. D **84** (2011) 016006.
G. Fejos and A. Hosaka, Phys. Rev. D **94** (2016) no.3, 036005.
- [19] P. Costa, M.C. Ruivo, and Yu.L. Kalinovsky, Phys. Lett. **B560**, 171 (2003).
- [20] H. Nagahiro, M. Takizawa and S. Hirenzaki, Phys. Rev. C **74** (2006) 045203.
Y. Kwon, S. H. Lee, K. Morita and G. Wolf, Phys. Rev. D **86** (2012) 034014
- [21] S. Sakai and D. Jido, Phys. Rev. C **88**, 064906 (2013).
- [22] S.D. Bass and A.W. Thomas, Phys. Lett. **B634**, 368 (2006).
- [23] K. Itahashi *et al.*, Prog. Theor. Phys. **128** (2012) 601.
- [24] M. Nanova *et al.* [CBELSA/TAPS Collaboration], Phys. Lett. B **727** (2013) 417.
- [25] M. Nanova *et al.* [CBELSA/TAPS Collaboration], Phys. Rev. C **94** (2016) no.2, 025205.
- [26] H. Nagahiro and S. Hirenzaki, Phys. Rev. Lett. **94**, 232503 (2005).
- [27] K. Saito, K. Tsushima and A. W. Thomas, Prog. Part. Nucl. Phys. **58** (2007) 1.
- [28] M. Miyatani, H. Nagahiro, S. Hirenzaki and N. Ikeno, Acta Phys. Polon. B **47** (2016) 367.
- [29] H. Nagahiro, S. Hirenzaki, E. Oset, and A. Ramos, Phys. Lett. **B709**, 87 (2012).
- [30] M. Nanova *et al.* [CBELSA/TAPS Collaboration], Phys. Lett. B **710** (2012) 600.
- [31] K. Kawarabayashi and N. Ohta, Prog. Theor. Phys. **66**, 1789 (1981).
- [32] S. D. Bass, Phys. Lett. B **463** (1999) 286.
- [33] B. Borasoy, Phys. Rev. D **61**, 014011 (2000).
- [34] E. Oset and A. Ramos, Phys. Lett. B **704**, 334 (2011).
- [35] S. Sakai and D. Jido, Hyperfine Interact. **234**, 71 (2015).

- [36] T. Sekihara, S. Sakai and D. Jido, Phys. Rev. C **94** (2016) no.2, 025203.
- [37] P. Moskal *et al.*, Phys. Lett. **B474**, 416 (2000).
P. Moskal *et al.*, Phys. Lett. **B482**, 356 (2000).
E. Czerwinski *et al.*, Phys. Rev. Lett. **113**, 062004 (2014)
- [38] P. G. Moyssides *et al.*, Nuovo Cim. A **75**, 163 (1983).
- [39] J. F. Zhang, N. C. Mukhopadhyay and M. Benmerrouche, Phys. Rev. C **52** (1995) 1134.
Z. p. Li, J. Phys. G **23** (1997) 1127.
B. Borasoy, Eur. Phys. J. A **9** (2000) 95.
S. D. Bass, S. Wetzell and W. Weise, Nucl. Phys. A **686** (2001) 429.
B. Borasoy, E. Marco and S. Wetzell, Phys. Rev. C **66** (2002) 055208.
W. T. Chiang, S. N. Yang, L. Tiator, M. Vanderhaeghen and D. Drechsel, Phys. Rev. C **68** (2003) 045202.
A. Sibirtsev, C. Elster, S. Krewald and J. Speth, AIP Conf. Proc. **717** (2004) 837.
K. Nakayama and H. Haberzettl, Phys. Rev. C **69** (2004) 065212.
K. Nakayama and H. Haberzettl, Phys. Rev. C **73** (2006) 045211.
V. A. Tryasuchev, Phys. Part. Nucl. **39** (2008) 64.
X. Cao and X. G. Lee, Phys. Rev. C **78** (2008) 035207.
F. Huang, H. Haberzettl and K. Nakayama, Phys. Rev. C **87** (2013) 054004.
- [40] M. Williams *et al.* [CLAS Collaboration], Phys. Rev. C **80** (2009) 045213.
- [41] P. Levi Sandri *et al.*, Eur. Phys. J. A **51** (2015) no.7, 77.
- [42] M. Sumihama *et al.* [LEPS Collaboration], Phys. Rev. C **80** (2009) 052201.
- [43] V. Crede *et al.* [CBELSA/TAPS Collaboration], Phys. Rev. C **80** (2009) 055202.
- [44] V. L. Kashevarov, L. Tiator and M. Ostrick, Bled Workshops Phys. **16** (2015) 9.
- [45] K. Kawarabayashi and M. Suzuki, Phys. Rev. Lett. **16** (1966) 255.
N. Fayyazuddin and N. Riazuddin, Nucl. Phys. **31** (1962) 649.
- [46] K. A. Olive *et al.* [Particle Data Group Collaboration], Chin. Phys. C **38** (2014) 090001.
- [47] S.L. Adler, Phys. Rev. **177**, 2426 (1969).
J.S. Bell and R. Jackiw, Nuovo Cim. A **60**, 47 (1969).
- [48] R. K. Rader *et al.*, Phys. Rev. D **6** (1972) 3059.
- [49] T. Hyodo, D. Jido and A. Hosaka, Phys. Rev. C **78**, 025203 (2008).

- [50] K. S. Choi, S. i. Nam, A. Hosaka and H. C. Kim, Phys. Lett. B **636** (2006) 253.
K. S. Choi, S. i. Nam, A. Hosaka and H. C. Kim, J. Phys. G **36** (2009) 015008.